PCCP

Accepted Manuscript

ROYAL SOCIETY OF CHEMISTRY

www.rsc.org/pccp

Three-dimensional sp^2-hybridized carbons consisting of orthogonal nanoribbons of graphene and net C

Meng Hu, Xu Dong, Bingchao Yang, Bo Xu, Dongli Yu and Julong He*

State Key Laboratory of Metastable Materials Science and Technology, Yanshan University, Qinhuangdao, 066004, China

* E-mail: hjl@ysu.edu.cn

Abstract

We identify two sp^2 hybridized network models of carbon, namely GT-8 and CT-12, based on first-principles calculation results. The parallel nanoribbon rows of graphene and net C are found to be interlinked with orthogonal nanoribbons to construct GT-8 and CT-12, and their series of isomorphic analogs (named GTs and CTs) assembled with the widening of nanoribbon components. GTs and CTs are dynamically and mechanically stable and energetically more favorable than many previous sp^2 carbons, including K_4, C20, and H6 carbon. They are two-dimensional conductors with insulating properties in the *z*-axis. Remarkably, GTs were superconductive with increased superconducting transition temperature T_c as nanoribbons widen. The T_c's of GT-8 and GT-16 are 5.2 and 14.0 K respectively, which are higher than that of boron-doped diamond under the same value of Coulomb pseudopotential μ^*. They possess higher bulk modulus than graphite and behave as excellent ductile materials. The Young's modulus of GT-8 along the *z*-axis is comparable with that of graphene and it significantly increases as nanoribbons widen.

Elemental carbon fosters numerous modifications owing to the versatile hybridization states by altering the periodic binding motif in networks consisting of sp^3-, sp^2-, and sp-hybridized carbon atoms. Intricate hybridization states determine the structural diversity and further contribute various intriguing properties for scientific and technological significance. Graphite, fullerenes, carbon nanotubes, and graphene are well-known manners that fill a space with only sp^2 carbon atoms. The discovery of fullerene C_{60} marks the beginning of an era of synthetic carbon allotropes; together with further developed carbon nanotubes and graphene, the allotropes overwhelmingly illustrate their unique charming properties including zero band-gap, ultrahigh Young's modulus and tensile strength, high thermal conductivity, and ballistic electron transport,[1-4] where the characteristics of sp^2 bonding has a decisive effect. Fullerenes, nanotubes, and graphene are the zero-, one-, and two-dimensional configurations of sp^2 carbon atoms, respectively. Considering the strict anisotropic characteristics of the three carbons for the limited structural dimensions, three-dimensional (3D) covalently bonded sp^2 carbons are proposed and expected to exhibit more amazing properties, such as high hardness and superconductivity.

Ample 3D sp^2-hybridized carbons have been theoretically constructed, including $ThSi_2$-structured bct-4, cubic K_4, C20, and sp^2-diamond, hexagonal H-6 and cH6 (or called 6(3)2-21 net), rhombohedral cR6 carbon (or called 6(3)2-22 net), tetragonal cT8 carbon, and triangular carbon exhibiting diverse distinguished properties.[5-11] For instance, K_4 and cH6 are metallic; sp^2-diamond is semiconductive with a direct band gap; cR6 and cT8 are also semiconductive but possess wider indirect band gaps and comparable bulk modulus with graphite; Young's modulus and bulk modulus of triangular carbon are higher than steel. 3D sp^2-hybridized carbons indicate that tunable electronic and mechanical properties can be realized in them although they are

usually energetically metastable relative to C_{60} or even dynamically unstable.[9, 12]

This work presents ab initio calculation designs of two tetragonal sp^2 hybridized carbon allotropes, GT-8 and CT-12, constructed by orthogonal nanoribbons of graphene and net C (a one-atom sheet composed of squares C_4, hexagons C_6, and octagons C_8). They meet the criteria of dynamical and mechanical stabilities and are energetically more stable than K_4, C20, H6, bct-4, and cH6; GT-8 possesses comparable energy with C_{60}. A series of isomorphic derivatives of GT-8 and CT-12 are constructed and named GTs and CTs, respectively, by widening nanoribbon constituents. Electronic band structure calculations imply that the superconductive characteristics of GTs and the application of the Allen-Dynes modified McMillan equation reveal their superconducting transition temperature of 5.2 K for GT-8 and 14.0 K for GT-16, which increase with the widening of nanoribbons. The Young's modulus of GTs in *z*-axis is higher than the in-plane modulus of graphite, and it increases remarkably as the nanoribbons widen. The Young's modulus in *x*- and *y*-axis also reaches about 0.7 TPa. The Young's modulus of CTs is weaker with respect to GTs for the introduction of large octagons.

2 Computational methods

Structural searches were conducted up to 24 atoms/cell in the 0 to 25 GPa pressure range using the well-developed CALYPSO code,[13, 14] which has successfully predicted many carbon allotropes.[15-17] Except the proposed GT-8 and CT-12, previous sp^2 carbons including bct-4, K_4, C20, sp^2-diamond, H-6, cH6, cR6, cT8 carbon, and triangular carbon, were reproduced in the crystal searching process. The underlying geometric optimization and electronic properties predictions were performed using density functional theory (DFT) as implemented in the VASP code.[18] The PAW[19] pseudopotential was used with $2s^22p^2$ as valence electrons of a carbon atom. The

exchange correlation terms were treated employing LDA[20, 21] at a converged plane-wave cutoff energy of 660 eV. The electronic band structures of GT-8 and CT-12 were revised by performing HSE06 hybrid functional[22] calculations, which provided a more accurate description of the exchange-correlation energy of electrons because DFT systematically underestimated the band gap of a semiconductor or an insulator or even incorrectly predict a metal. The phonon frequencies of the structures were calculated using the finite displacement method as implemented in CASTEP code,[23] and the optimized structures from VASP are optimized again using CASTEP code before phonon calculations. Primitive cells were used to calculate the elastic constants, bulk modulus, shear modulus, and Young's modulus using CASTEP code.[23] The electron-phonon coupling (EPC) was computed using the Quantum-ESPRESSO package[24] with plane-wave pseudopotential method and density functional perturbation theory (DFPT).[25, 26] The ultrasoft pseudopotential within PBE was used at a tested kinetic energy cutoff of 50 Ry.

3 Results and discussion

GT-8 with 8 carbon atoms in a tetragonal cell was assembled with the narrowest zigzag-edged graphene nanoribbons (GNRs). In GT-8 (Fig. 1a), vertical aligned GNR arrays (the blue sections) were interlinked to the horizontal arrays (the olive sections) with a dihedral angle of 90° accompanied by the edge dangling bonds spontaneously establishing sp^2 buckles. Two kinds of bond angles of 123.49° and 118.25° existed in GT-8, approaching the standard sp^2 hybridization angle in graphene and graphite (120°). The C-C bond lengths (Fig. 2a) of inner ribbons are 1.427 and 1.429 Å, and the bonds jointing the two orthogonal ribbons were stretched to 1.477 Å, which were slightly larger than that of graphite and graphene (1.412 Å). The lengthened C-C bonds (1.477 Å) originate from that the two sp^2-carbons are rotated by 90° and then

their free *p*-orbitals are orthogonal to one another without overlap, which disrupts the conduction pathway along the *z* direction (see detailed discussion below). The local atomic environment is similar to an ethylene molecule at excited state which undergoes rotation forming a perpendicular configuration featuring an elongated C-C bond.[27] The electron localization function (ELF), a simple measure of electron localization in atomic and molecular systems,[28] was calculated to qualitatively describe the bonding characteristics. As depicted in Fig. 2, ELF analysis showed that the C-C bonds in GT-8 features π state, which coincided with the bond lengths and angles distribution.

CT-12 was built by a similar fashion as GT-8, but the orthogonal nanoribbons were substituted with nanoribbons of net C, which contained squares C_4, hexagons C_6 and octagons C_8 and has stimulated great research interest for its intriguing properties (Fig. 1b).[29] The special configuration of net C expanded the bond angle ranges from 90° to 145.22° and bond length 1.387 Å to 1.450 Å in CT-12; however, the C-C bonds were still in sp^2 hybridization from ELF results (Fig. 2b). The crystal structure parameters and densities of GT-8 and CT-12 were shown in Table 1. The distances between parallel nanoribbons in GT-8 and CT-12 were 2.518 and 3.728 Å, respectively, and that of graphite (3.35 Å) was between them. Therefore, the density of GT-8 reached about 80% that of a diamond (3.63 g/cm^3), whereas CT-12 was looser than graphite (2.301 g/cm^3).

Apparently, the configuration features of GT-8 and CT-12 determined that plenty of isomorphic analogs (termed as GTs and CTs, respectively) were assembled with expanding the nanoribbons width. Two representatives, GT-16 (16 carbon atoms in a tetragonal cell) and CT-24 (24 carbon atoms in a tetragonal cell) with doubled ribbon widths relative to GT-8 and CT-12 are presented in Fig. 1 and Table 1. The isomorphic

analogs had similar inter-nanoribbon vertical distances and densities with GT-8 and CT-12, respectively. The broad and connected tunnels in GTs and CTs were ready to accommodate and filter little molecules and ions to act as molecular sieve, catalyst carrier, shape-selective catalysts, and absorbent.

The phonon dispersions and elastic constants were calculated to check the crystal structural stabilities of GT-8 and CT-12. As shown in Fig. 3a, no imaginary phonon frequency was observed throughout the whole Brillouin zone, indicating the dynamical stabilities of the two carbons. The calculated independent elastic constants (Table 2) satisfied the generalized Born stability criteria,[30] suggesting that they were mechanically stable at ambient pressure. In addition, the formation energies (normalized to per carbon) of GTs and CTs were contrasted with graphene, C_{60} and some other sp^2 carbon allotropes (Fig. 3b). GTs and CTs were energetically metastable relative to graphene but more favorable than K_4, C20, H6, cH6, and cR6. GT-8 had comparable energetically stability with C_{60}, and wider nanoribbon assembled GTs were more stable than C_{60}. The squares and octagons of net C introduced great stress into CTs, resulting in lower thermodynamic stability. As LDA tends to overbind systems where van der Waals interactions exist, the TS+SCS method,[31, 32] which can well reproduce the structure and interlayer binding energy of graphite,[33] as implemented in the VASP code are used to optimize the geometries and compare the relative energies of GT-8, CT-12, and graphite. The calculated energies of GT-8 and CT-12 relative to graphite are 0.417 and 0.544 eV/atom respectively, which are similar to the LDA results (0.421 and 0.548 eV/atom) and further confirm the high stabilities of GTs and CTs.

The electronic band structures of GT-8 and CT-12 were calculated using the HSE06 functional[22] as illustrated in Fig. 4. Both carbons exhibited metallic properties.

Band decomposed charge density around the Fermi level were delineated to clear the conductive direction (Fig. 4). Band decomposed charge analysis indicated that the electrons distribution on GTs accurately spread around the hexagons and expanded in the longitudinal direction without the influence of interlinked orthogonal nanoribbons. Accordingly, GTs showed the strongest electric conduction along the *x* and *y* directions but were insulated in the *z*-axis in line with the insulation feature along the Γ–Z line shown in the band structure, which has to do with the orthogonal *p*-orbitals between neighboring constituent nanoribbons (see above). Obviously, the planar conductivity in the direction between *x*- and *y*-axis regularly changed from strongest (*x*-axis) to weak and strongest (*y*-axis) again, which was important for nanoelectronic switch. Similar features were discovered in CT-12 and CT-24 whose conduction pathway were also interrupted in the *z*-axes and showed planar conduction pathway. However, the distance between nanoribbons in CT-12 and CT-24 was larger than the interlayer distance of graphite. Thus the interaction between the 2*p* electrons of nanoribbons became forbidden and with weaker conductivity. Recent investigations indicate that edge-modified GNRs present antiferromagnetic edge magnetization,[34, 35] however, no magnetism is found in GTs and CTs by calculating the spin polarized projected density of states (PDOS).

Band structure calculations on GT-8 and GT-16 declared that the band along the R-X of Brillouin zone (the red line in Fig. 4a) was quite flat and feature a "flat band-steep band" character,[36] which suggested superconductive potential. The superconducting transition temperature T_c was estimated employing the Allen and Dynes modified McMillan equation,[37] $T_c=\frac{\omega_{log}}{1.2}\exp[-\frac{1.04(1+\lambda)}{\lambda-\mu^*(1+0.62\lambda)}]$, where ω_{log} is the logarithmic average frequency, λ is the EPC coefficient, and μ^* is the Coulomb pseudopotential. The calculated EPC coefficient λ in Table 3 was 0.42 for GT-8 and

1.20 for GT-16, which indicates that the EPC of GT-16 was much stronger than GT-8. Previous calculations showed that μ^*=0.1 is necessary to achieve excellent agreement with the experimental result in estimating the T_c of boron-doped diamond.[38] Under the same value of Coulomb pseudopotential, T_c of 5.2 K for GT-8 and 14.0 K for GT-16 were obtained, which confirmed their superconductivities and present higher T_c than that of boron-doped diamond (4.4 K). It is noted that wider graphene nanoribbon assembled GTs present higher superconducting transition temperature.

The bulk modulus and shear modulus of graphite were 142.3 and 108.0 GPa, respectively, which originated from the weak linkages between graphene sheets. The bulk moduli of GT-8 and GT-16 (Table 4) were twice as much as that of graphite and about 80% that of diamond. The bulk moduli of CT-12 and CT-24 are decreased to about 200 GPa as larger porous structures were introduced. The shear modulus of GTs was higher than that of graphite, whereas that of CTs reduced to half of graphite. The structures easily slipped for the deformable sp^2 buckling. Pugh[39] proposed that the ratio of B/G was used to qualitatively describe the brittle or ductile behavior of a material, where a high (low) B/G value was often associated with ductility (brittleness), and the critical value that differentiated ductile and brittle material was 1.75. The value of diamond was 0.8, rendering a strong brittle property. GTs and CTs were both excellent ductile materials with high ratio values of 2.6 to 4.0. GTs and CTs assembled with wider nanoribbons showed similar bulk and shear moduli with GT-8 and CT-12, respectively, such as calculated bulk modulus of 346.0 GPa for GT-32 with four times nanoribbon width relative to GT-8.

Carbon nanotubes and graphene were quite stiff along their expanding direction and the Young's modulus reached about 1 TPa.[4, 40] As shown in Fig. 1, orthogonal nanoribbons in GTs and CTs were both parallel to *z*-axis, whereas *x*-axis or *y*-axis was

the expanding direction of half nanoribbons. The Young's moduli Y_z of GTs (Table 4) were comparable to that of graphene and Y_x and Y_y also reached higher than 0.7 TPa, whereas that of CTs were lower for large octagons holes. Different from the tendency of bulk modulus and shear modulus, the Young's moduli of both structures were significantly strengthened as the nanoribbon widened, which had been proved that the Young's modulus of graphene nanoribbons depended strongly on size.[41]

4 Conclusions

Two sp^2 carbon allotropes, termed as GT-8 and CT-12, composed of orthogonal nanoribbons of graphene and net C were proposed based on first principles calculations. There are a series of isomorphic analogs, named GTs and CTs, identified through broadening the nanoribbon width. They were mechanically and dynamically stable and energetically more stable than many recently predicted sp^2 carbon, including K_4, C20, H6, cH6, and cR6. Band structure calculations showed that both carbons were metallic, and band decomposed charge density analysis indicated their planar conductivity. GTs were superconductive with superconducting transition temperature of 5.2 K for GT-8 and 14.0 K for GT-16. GTs and CTs possessed higher bulk modulus than graphite, and showed excellent ductile properties. Young's modulus of GTs reached higher than 1 TPa, which was comparable to graphene, and it increased significantly as the nanoribbons widened.

Acknowledgements

This work was supported by the National Science Foundation of China (Grants Nos. 51421091, 51332005, and 5127222), the National Basic Research Program of China (Grant No. 2011CB808205) and the Natural Science Foundation for Distinguished

Young Scholars of Hebei Province of China (E2014203150). The authors acknowledge Ph. D. Zhisheng Zhao for help in discussing the crystal structures.

References

1 A. Hirsch, *Nat. mater.*, 2010, **9**, 868.
2 I. Sumio, *Nature*, 1991, **354**, 56.
3 K. S. Novoselov, A. K. Geim, S. V. Morozov, D. Jiang, Y. Zhang, S. V. Dubonos, I. V. Grigorieva and A. A. Firsov, *Science*, 2004, **306**, 666.
4 M. M. J. Treacy, T. W. Ebbesen and J. M. Gibson, *Nature*, 1996, **381**, 678.
5 R. Hoffmann, T. Hughbanks, M. Kertesz and P. H. Bird, *J. Am. Chem. Soc.*, 1983, **105**, 4831.
6 A. Y. Liu and M. L. Cohen, *Phys. Rev. B*, 1992, **45**, 4579.
7 M. Côté, J. C. Grossman, M. L. Cohen and S. G. Louie, *Phys. Rev. B*, 1998, **58**, 664.
8 M. Itoh, M. Kotani, H. Naito, T. Sunada, Y. Kawazoe and T. Adschiri, *Phys. Rev. Lett.*, 2009, **102**, 055703.
9 J. T. Wang, C. Chen and Y. Kawazoe, *Sci. Rep.*, 2013, **3**, 3077.
10 B. Winkler, C. J. Pickard, V. Milman and G. Thimm, *Chem. Phys. Lett.*, 2001, **337**, 36.
11 M. Wu, X. Wu, Y. Pei, Y. Wang and X. C. Zeng, *Chem. Commun.*, 2011, **47**, 4406.
12 V. V. Brazhkin and A. G. Lyapin, *Phys. Rev. Lett.*, 2000, **85**, 5671.
13 Y. Wang, J. Lv, L. Zhu and Y. Ma, *Phys. Rev. B*, 2010, **82**, 094116.
14 Y. Wang, J. Lv, L. Zhu and Y. Ma, *Comput. Phys. Commun.*, 2012, **183**, 2063.
15 M. Hu, F. Tian, Z. Zhao, Q. Huang, B. Xu, L.-M. Wang, H.-T. Wang, Y. Tian and J. He, *J. Phys. Chem. C*, 2012, **116**, 24233.
16 M. Hu, X. Dong, Y. Pan, B. Xu, D. Yu and J. He, *J. Phys.: Condens. Matter*, 2014, **26**, 235402.
17 Z. Zhao, F. Tian, X. Dong, Q. Li, Q. Wang, H. Wang, X. Zhong, B. Xu, D. Yu, J. He, H.-T. Wang, Y. Ma and Y. Tian, *J. Am. Chem. Soc.*, 2012, **134**, 12362.
18 G. Kresse and J. Furthmüller, *Phys. Rev. B*, 1996, **54**, 11169.
19 P. E. Blöchl, *Phys. Rev. B*, 1994, **50**, 17953.
20 D. M. Ceperley and B. J. Alder, *Phys. Rev. Lett.*, 1980, **45**, 566.
21 J. P. Perdew and A. Zunger, *Phys. Rev. B*, 1981, **23**, 5048.
22 J. Heyd, G. E. Scuseria and M. Ernzerhof, *J. Chem. Phys.*, 2003, **118**, 8207.
23 S. J. Clark, M. D. Segall, C. J. Pickard, P. J. Hasnip, M. I. J. Probert, K. Refson and M. C. Payne, *Z. Kristallogr.*, 2005, **220**, 567.
24 P. Giannozzi, S. Baroni, N. Bonini, M. Calandra, R. Car, C. Cavazzoni, D. Ceresoli, G. L. Chiarotti, M. Cococcioni, I. Dabo, A. Dal Corso, S. de Gironcoli, S. Fabris, G. Fratesi, R. Gebauer, U. Gerstmann, C. Gougoussis, A. Kokalj, M. Lazzeri, L. Martin-Samos, N. Marzari, F. Mauri, R. Mazzarello, S. Paolini, A. Pasquarello, L. Paulatto, C. Sbraccia, S. Scandolo, G. Sclauzero, A. P. Seitsonen, A. Smogunov, P. Umari and R. M. Wentzcovitch, *J. Phys.: Condens. Matter*, 2009, **21**, 395502.
25 S. Baroni, P. Giannozzi and A. Testa, *Phys. Rev. Lett.*, 1987, **58**, 1861.
26 P. Giannozzi, S. de Gironcoli, P. Pavone and S. Baroni, *Phys. Rev. B*, 1991, **43**, 7231.
27 M. Barbatti, J. Paier and H. Lischka, *J. Chem. Phys.*, 2004, **121**, 11614.
28 A. D. Becke and K. E. Edgecombe, *J. Chem. Phys.*, 1990, **92**, 5397.

29 N. Tyutyulkov, F. Dietz, K. Müllen and M. Baumgarten, *Chem. Phys. Lett.*, 1997, **272**, 111.
30 J. F. Nye, *Physical Properties of Crystals* Oxford University Press, Oxford, 1985.
31 A. Tkatchenko, R. A. DiStasio, R. Car and M. Scheffler, *Phys. Rev. Lett.*, 2012, **108**, 236402.
32 T. Bučko, S. Lebègue, J. Hafner and J. G. Ángyán, *Phys. Rev. B*, 2013, **87**, 064110.
33 V. V. Gobre and A. Tkatchenko, *Nat Commun*, 2013, **4**, 2341.
34 K. Kusakabe and M. Maruyama, *Phys. Rev. B*, 2003, **67**, 092406.
35 H. Lee, Y.-W. Son, N. Park, S. Han and J. Yu, *Phys. Rev. B*, 2005, **72**, 174431.
36 A. Simon, *Angew. Chem. Int. Ed. Engl.*, 1997, **36**, 1788.
37 P. B. Allen, *Phys. Rev. B*, 1975, **12**, 905.
38 H. J. Xiang, Z. Li, J. Yang, J. G. Hou and Q. Zhu, *Phys. Rev. B*, 2004, **70**, 212504.
39 S. F. Pugh, *XCII. Relations between the elastic moduli and the plastic properties of polycrystalline pure metals*, Taylor & Francis, 1954.
40 C. Lee, X. Wei, J. W. Kysar and J. Hone, *science*, 2008, **321**, 385.
41 H. Zhao, K. Min and N. Aluru, *Nano Lett.*, 2009, **9**, 3012.

Table and Figure captions

Table 1. The space group (S. G.), cell parameters (Å), atomic Wyckoff positions, and density (g/cm^3) of GTs and CTs at ambient pressure.

Table 2. Calculated elastic constants (C_{ij}, GPa) of GTs and CTs at ambient pressure.

Table 3. EPC coefficient λ, logarithmically averaged characteristic phonon frequency ω_{log}, and superconducting transition temperature T_c at zero pressure for GT-8 and GT-16.

Table 4. The calculated bulk modulus (B, GPa), shear modulus (G, GPa), ratio of B/G, and Young's modulus (Y_x, Y_y, Y_z, GPa) of graphite, diamond, GTs and CTs at ambient pressure.

Fig. 1 Crystal structures of (a~d) GT-8, CT-12, GT-16 and CT-24.

Fig. 2 Isosurface of ELF for GT-8 (a) and CT-12 (b) with the value of 0.75.

Fig. 3 (a) Phonon dispersion curves of GT-8 and CT-12 at ambient pressure. (b) Calculated formation energies of GTs, CTs, and other sp^2 carbon allotropes at ambient pressure. GTs: GT-8, GT-16, GT-24, GT-32, GT-40, GT-48, GT-56. CTs: CT-12, CT-24, CT-36, CT-48, CT-60, CT-72, CT-84.

Fig. 4 (a~b) Calculated electronic band structures of GT-8 and CT-12 using the HSE06 functional at ambient pressure. (c~f) Isosurfaces of band decomposed charge density around the Fermi level for GT-8, GT-16, CT-12 and CT-24, respectively.

Table 1. The space group (S. G.), cell parameters (Å), atomic Wyckoff positions, and density (g/cm^3) of GTs and CTs at ambient pressure.

Structure	S. G.	a	c	Atomic positions	Density
GT-8	P42/mmc	2.518	8.513	4g (0, 0, 0.3367) 4i (1/2, 0, 0.9162)	2.956
GT-16	P42/mmc	2.523	16.938	4g (0, 0, 0.2936) 4g (0, 0, 0.0417) 4i (1/2, 0, 5/6) 4i (0, 1/2, 0.5825)	2.960
CT-12	P42/mmc	3.728	8.976	8o (0, 0.3055, 0.0804) 4g (0, 0, 0.1685)	1.918
CT-24	P42/mmc	3.721	17.953	8o (0.6936, 0, 0.4155) 8o (0.3055, 0, 0.3350) 4g (0, 0, 0.2092) 4g (0, 0, 0.4601)	1.926

Table 2. Calculated elastic constants (C_{ij}, GPa) of GTs and CTs at ambient pressure.

structure	C_{11}	C_{33}	C_{44}	C_{66}	C_{12}	C_{13}	C_{16}
GT-8	728.6	1213.0	73.4	24.0	71.4	104.7	0.0
GT-16	741.2	1287.2	99.5	16.4	59.1	87.4	0.0
CT-12	392.4	632.4	47.1	0.8	16.9	113.7	0.0
CT-24	384.9	653.3	63.5	0.7	21.0	116.8	0.0

Table 3. EPC coefficient λ, logarithmically averaged characteristic phonon frequency ω_{log}, and superconducting transition temperature T_c at zero pressure for GT-8 and GT-16.

Structure	λ	ω_{log} (K)	T_c (K)	
			u^*=0.08	u^*=0.1
GT-8	0.42	913.6	7.7	5.2
GT-16	1.20	156.5	15.1	14.0

Table 4. The calculated bulk modulus (B, GPa), shear modulus (G, GPa), ratio of B/G, and Young's modulus (Y_x, Y_y, Y_z, GPa) of graphite, diamond, GTs and CTs at ambient pressure.

structure	B	G	B/G	Y_x, Y_y, Y_z
graphite	142.3	108.0	1.3	Y_x=Y_y=1011.4, Y_z=10.1
diamond	454.5	545.5	0.8	Y_x=Y_y=Y_z=1062.4
GT-8	348.5	130.4	2.7	Y_x=Y_y=714.1, Y_z=1185.6
GT-16	347.6	135.1	2.6	Y_x=Y_y=731.4, Y_z=1268.1
CT-12	201.4	50.4	4.0	Y_x=Y_y=371.9, Y_z=569.3
CT-24	202.9	53.5	3.8	Y_x=Y_y=364.0, Y_z=586.1

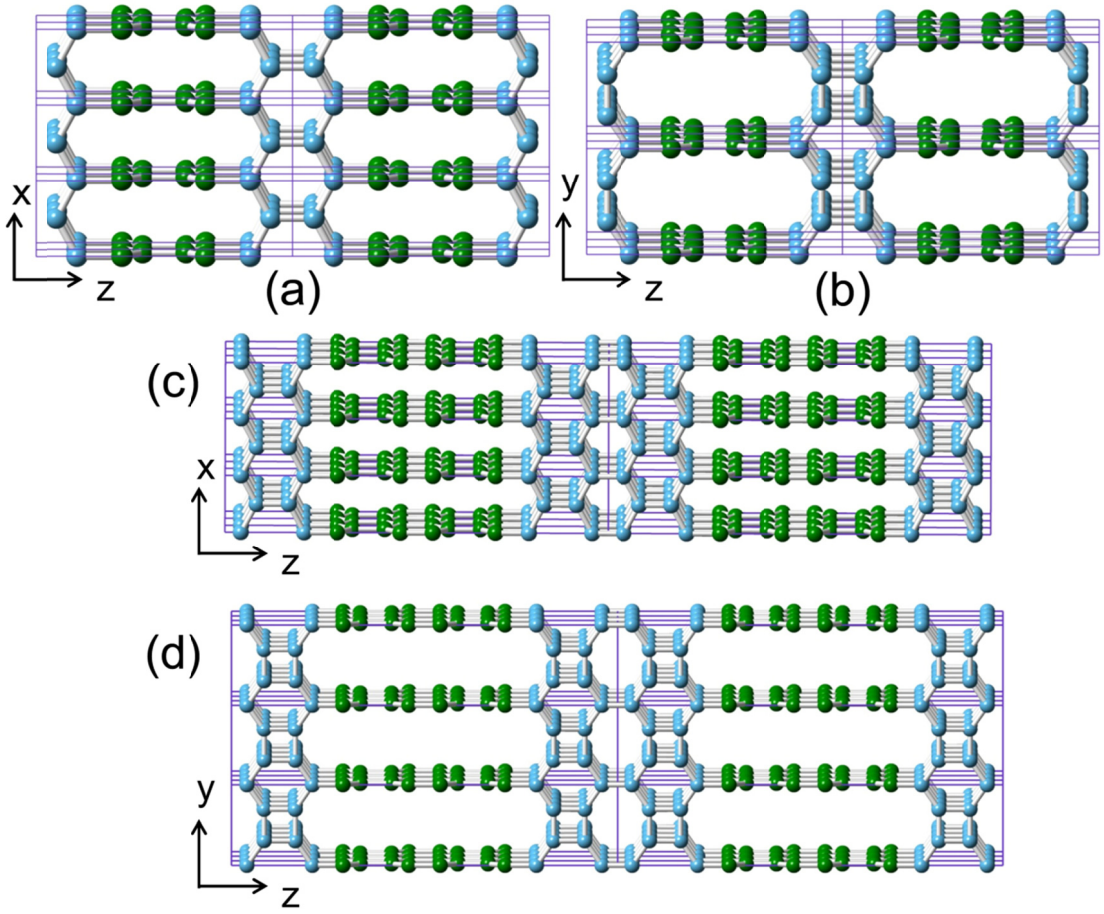

Fig. 1

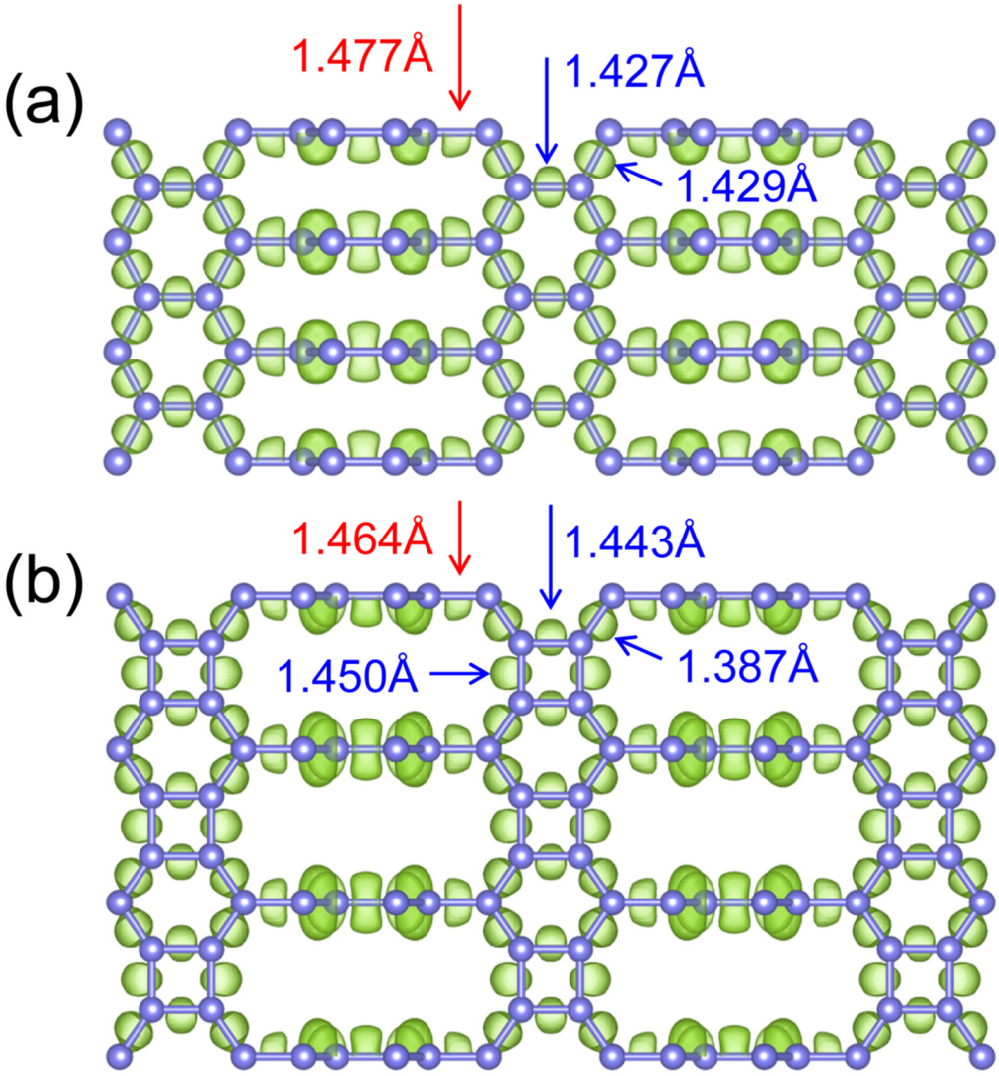

Fig. 2

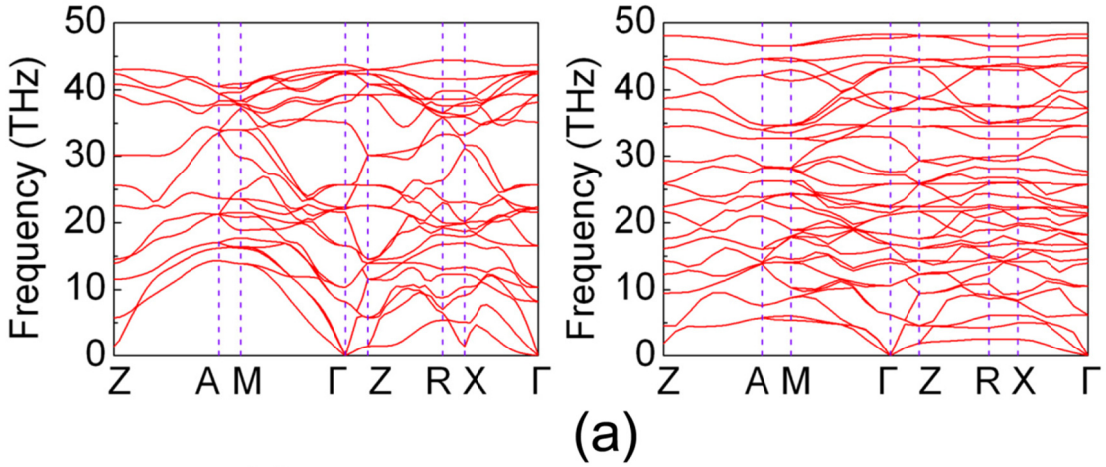

(a)

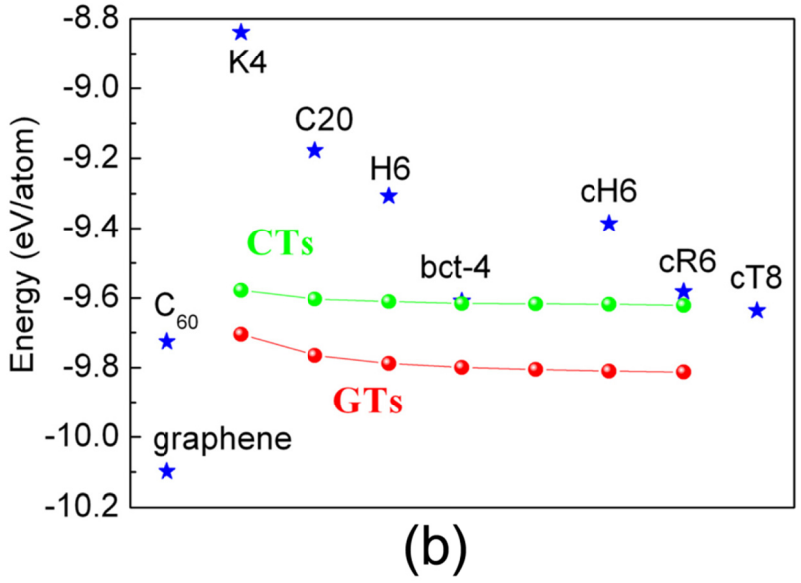

(b)

Fig. 3

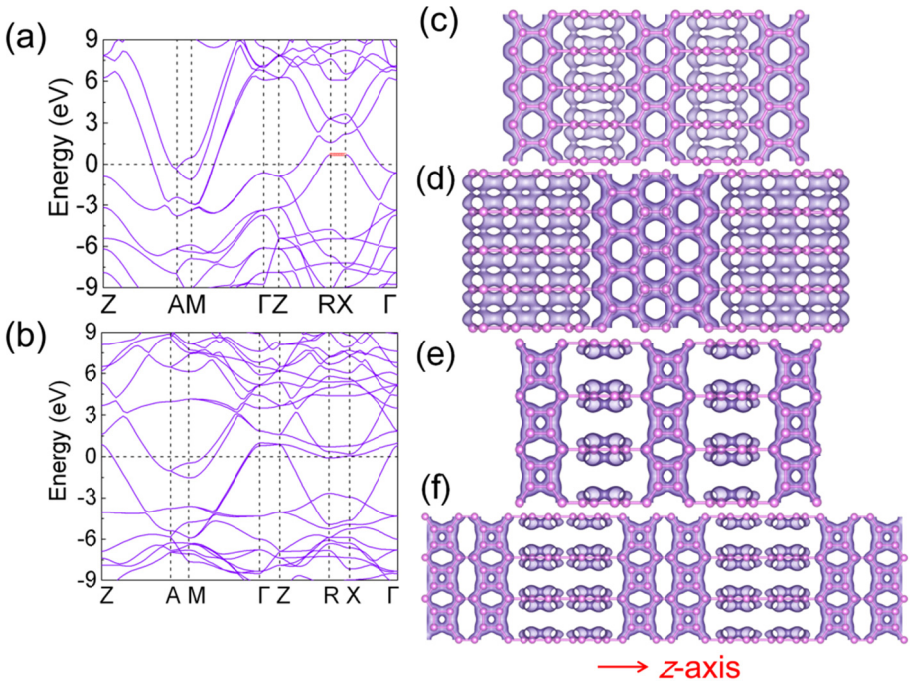

Fig. 4